Azzola *et al. Geothermal Energy* (2023) 11:30
https://doi.org/10.1186/s40517-023-00272-4

Geothermal Energy

RESEARCH Open Access

Integration of distributed acoustic sensing for real-time seismic monitoring of a geothermal field

Jérôme Azzola[1*], Katja Thiemann[2] and Emmanuel Gaucher[1]

*Correspondence:
jerome.azzola@kit.edu

[1] Institute of Applied Geosciences (AGW), Karlsruhe Institute of Technology (KIT), Karlsruhe, Germany
[2] Stadtwerke München GmbH, Munich, Germany

Abstract

To accelerate the energy transition, the exploitation of deep geothermal reservoirs is becoming a priority to supply district heating networks in areas with high potential for geothermal applications. However, the sustainable development of the resource exploitation implies minimizing the associated risks, in particular related to induced seismicity, while optimizing operational processes. Besides, the growth of this energy sector, often supported by financial aid programs, provides resources to the industry that were not available in the past to implement advanced monitoring strategies. In this context, we present a monitoring system establishing Distributed Acoustic Sensing (DAS) as an effective component of the seismic network used for the monitoring of the geothermal field of Schäftlarnstraße (Munich, Germany). We also investigate its potential for real-time seismic monitoring in an urban environment and for risk mitigation. The monitoring system is based on a data management system linking the on-site acquisition infrastructure, including the fiber optic cable deployed in an injection well and the associated DAS interrogator, to a cloud Internet-of-Things (IoT) platform. The latter is designed to deliver both a secure storage environment for the DAS recordings and optimized computing resources for their processing. The proposed solution has been tested over a six-month period under operating conditions of the geothermal field. The survey proves the feasibility of efficiently acquiring and processing the large flow of continuous DAS data. The processing outcomes, emphasized by two detected local seismic events, demonstrate the suitability of DAS, cemented behind the casing of a flowing well, for (micro-) seismic monitoring of the geothermal site. The processing applied to the data takes advantage of the high spatial density of the acquisitions for their de-noising and for the detection of events. We find that the DAS monitoring system is capable of successfully detecting an event that could not be detected by the standard surface or shallow-borehole 3C-seismometers, despite noisy conditions associated with the urban environment and the field operation. The six-month test period demonstrates the potential of DAS to be integrated as a routine seismic monitoring component of an operating geothermal field. In addition, it highlights its advantageous role as a complement to surface seismometer-based networks, particularly in urban environments.

Keywords: Distributed Fiber Optic Sensing (DFOS), Cloud-computing, Reservoir management, Deep geothermal, Molasse Basin, Munich

Introduction

In order to accelerate the energy transition and to reduce dependency on energy supply, the European community and several of its countries (e.g. France, Germany) are presently supporting the use of geothermal energy, especially for heat supply. In the Greater Munich area (Germany), this source of energy has been exploited with considerable success since the late 1990s (Agemar et al. 2014; Dussel et al. 2016). Indeed, the Malm carbonates formed during the Upper Jurassic period present favorable characteristics for heat extraction and possibly electricity generation, serving as the primary geothermal reservoir within the Molasse basin (Schulz and Jobmann 1989; Agemar et al. 2012). As part of the ongoing effort to adopt renewable energy sources, several projects are developed to further exploit this resource in the Munich area. Thus, Stadtwerke München GmbH (SWM), the energy provider of the Munich city, is planning several additional doublets (Cröniger et al., 2022), a development which is part of their strategy to cover 100% of the district heating demand with CO2-neutral resources by 2040, at the latest. The intensification of the resource exploitation therefore requires, more than ever, sustainable development and operation of the geothermal fields, which implies minimization of all associated risks, not only geological or economical, but also related to induced seismicity.

Exploiting deep geothermal reservoirs changes the original stress state prevailing in the subsurface. Observations and analyses show that these perturbations can induce seismicity, not only in so-called enhanced geothermal systems, but also in hydrothermal systems driven by a porous matrix (Kraft et al. 2009; Seithel et al., 2019; De Santis et al. 2022). This applies also to low-seismic-hazard environments such as the Munich area. Indeed, Megies and Wassermann (2014) demonstrated that even non-pressure-stimulated geothermal reservoirs with good hydraulic parameters are likely to cause seismicity. Hence, the increasing number of deep geothermal plants in the urban environment of the Greater Munich area calls for dedicated local seismic monitoring to complement the existing public monitoring (e.g. Azzola et al. 2021). It also requires the development of tailored and optimized monitoring strategies to acquire, process and distribute seismic recordings and the associated results to the field operators (Bohnsack et al. 2023). The full integration of monitoring strategies into the geothermal field operation could promote safe and sustainable management of the geothermal resource, especially if monitoring outcomes feed numerical models aiming at forecasting the thermo-hydro-mechanical response of the geothermal system to the operational conditions (e.g. Gaucher et al. 2015; Grigoli et al. 2017).

In this political and economic context, geothermal operators benefit from a greater investment capacity than in the past to develop solutions to meet this need in monitoring strategies. For instance, Distributed Optical Fiber Sensors (DOFS) technologies, well known from the oil and gas industry, is increasingly being adopted by the geothermal sector to assess the benefits for their own application and specificities (e.g. well completion, circulating fluid properties, fluid flow rates). The operating principle behind fiber optic sensing (see e.g. Hartog (2017) for an extensive review on the associated technologies) is based on the use of an optoelectronic system delivering spatially resolved measurements along the optical fiber to which it is connected. The elastic scattering of photons along the optical fiber make it possible to acquire various physical parameters

such as changes in dynamic strain (Distributed Acoustic Sensing, DAS), changes in static strain (Distributed Strain Sensing, DSS) and changes in temperature (Distributed Temperature Sensing, DTS) along its length. For monitoring applications, a significant advantage lies therefore in the possibility of acquiring DTS, DSS and DAS with one single fiber optic cable (FOC) composed of several fiber types. Applied to the oil and gas industry, Koelman et al. (2012) and Van Der Horst et al. (2013) discuss field trials combining different DOFS technologies in borehole acquisition. They demonstrate the potential of the technology for a range of applications, from temperature or flow profiling to the monitoring of well completion and induced seismicity, while highlighting the challenges associated with the data flow management. This makes DOFS an attractive tool to better characterize and monitor geothermal reservoirs too.

DAS, which is the focus of this article, has developed in the last decades as a geophysics instrument and has been applied in seismic analysis with established quality and performance (e.g. Parker et al., 2014; Lindsey et al., 2020; Paitz et al. 2021). In the field of borehole seismic acquisitions, applications are as varied as production control, well integrity supervision or seismic monitoring (see Johannessen et al., 2012; Parker et al., 2014; Li et al. 2015; Li et al. 2021 for reviews on possible applications). DAS technology gained early acceptance in the oil and gas industry (Baldwin, 2014, 2018) and demonstrated great potential as a long and dense seismic antenna, for instance in vertical seismic profiling (Madsen et al. 2012; Mateeva et al. 2012; Harris et al., 2016; Miller et al., 2016). The potential for time-lapse monitoring of reservoirs was also demonstrated (e.g. Mateeva et al., 2014). Furthermore, the high temporal and spatial sampling of DAS data allows fine resolution of local changes along boreholes, which applies for example to the identification of fluid-entry points and the quantification of production zones (Naldrett et al. 2018).

For seismic monitoring, DAS has shown great success in capturing signals in a wide range of magnitudes, e.g. microseismic or teleseismic events (Lellouch et al. 2020; Ajo-Franklin et al. 2019). In geo-reservoir applications, DAS along borehole brings sensors closer to the reservoir than surface seismometers, thus closer to the seismicity potentially induced by the exploitation of the resource. Consequently, borehole DAS may significantly contribute to the seismic monitoring provided the FOC is properly coupled to the ground and the well does not act as a permanent noise source (e.g. Li et al. 2018; Lellouch et al. 2019; Pankow et al. 2020). The un-aliased spatial sampling achieved with DAS also allows for improved visualization of seismic signals and access to a range of processing approaches usually applied in active seismic or large-array seismology for data de-noising and event detection.

In order to assess the capabilities of DAS (and DTS) technology, two wells of the newly developed geothermal field in Schäftlarnstraße (SLS), in the Munich city, have been equipped with FOCs [see Fig. 1 (a)]. At the SLS site, the amount of data to be collected with this DAS equipment goes up to several tens of megabytes per second. The collection and timely processing of this data flow may constitute a hindrance to the integration of the monitoring results into the operation of the geothermal field, especially when considering all aspects of the data handling, including secure and remote access to the recordings. Hence, an appropriate data management and processing infrastructure is necessary for the DAS system to constitute a real-time

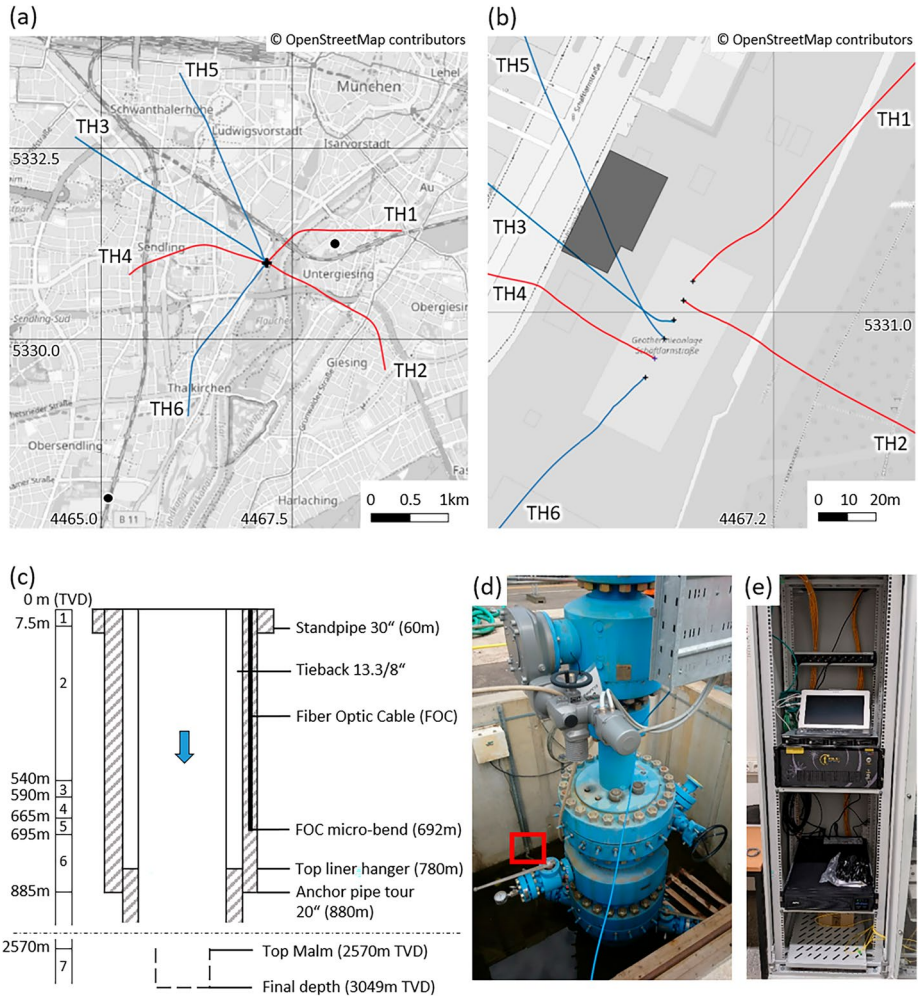

Fig. 1 Overview of the study site. Panel (**a**) location of the geothermal field in the southern part of Munich city and projection on the surface of the trajectory of the six wells. Red lines denote production wells and blue lines show injection wells. The black dots show the location of the two nearest seismic monitoring stations, which are two borehole 3C-seismometers located to the East and to the Southwest of the SLS site. The Gauss-Kruger 4 coordinate system is used for the Northing and Easting markers. Panel (**b**) focus on the Schäftlarnstraße geothermal field. The gray polygon shows the location of the control room in which the Febus A1-R interrogator and recording system was installed on the well site. Panel (**c**) completion of the injection well TH3 along its first 900 m (top) and in the open-hole section, until final depth (bottom). The arrow highlights the flow direction. The TH3 FOC, which is the focus of the study, is cemented behind casing. The installation allows the section to be interrogated twice, since the FOC forms a U-loop with a micro-bend located at a depth of 692 m (TVD). The well is vertical in the section of interest. The FOC faces on one side a tieback filled with annulus fluid and on the other side, the shallow sedimentary layers of the Molasse basin. The column on the left shows the stratigraphy. Numbers 1 to 7 refer respectively to "Quaternary", "Obere Süßwasser Molasse (OSM)", "Süßbrackwasser Molasse (SBM)", "Obere Meeresmolasse (OMM) Glaukonit Sande", "OMM Blättermergel", "OMM Neuhofener Schichten", "Upper Jurassic (Malm) carbonate formation". Panel (**d**) picture of the TH3 wellhead. The red rectangle highlights the entry point of the FOC in the ground, next to the location where the FOC was tapped to calibrate the position of the measuring points. Panel (**e**) picture of the setup in the control room. It shows the DAS interrogator, the Uninterrupted Power Supply (UPS) and the peripheral devices, which are all secured in a metallic enclosure

continuous component of the geothermal site monitoring. In this paper, we demonstrate the technical feasibility of implementing a DAS-based continuous and permanent seismic monitoring in the operational environment of the SLS geothermal field. This can constitute a proof of concept for future implementation in operational

geothermal contexts and a first step to make DAS-based seismic results a standard component of geothermal reservoir monitoring systems.

Sect. "The DAS monitoring system" of the manuscript presents the concept that was developed to interconnect the DAS interrogator and a cloud based internet-of-things (IoT) platform in order to manage the different phases of the monitoring, from the acquisition to the archiving and the processing of the DAS data. It has been designed to be integrated into the operator's management system and efficiently meet requirements in terms of processing capacities, storage volumes, access right delegation and scalability. In Sect. "Data processing workflows", we focus on the data processing and describe the workflow that was implemented on cloud-workstations to screen the data for possible local induced seismicity. We provide insights into the recording conditions and the de-noising strategies applied to enhance the signal of interest and achieve a satisfactory level of detection. The results of the six-month continuous acquisition period, aimed at assessing the capabilities of the concept from February to July 2022, are described in Sect. "Monitoring results" To evaluate the performance of the monitoring system, we focus on two local microseismic events that were detected by the proposed monitoring system. The results of this trial period are discussed in Sect. "Discussion". We first concentrate on the utilization of DAS in the routine operation of the geothermal field, considering the monitoring capabilities demonstrated at the SLS site. We then elaborate on the potential of the proposed concept for real-time seismic monitoring of geothermal fields and discuss possibilities in terms of scaling up. In this regard, we present how the monitoring concept can contribute to the development of a reservoir management system, with the goal of providing ongoing guidance to the operator for the efficient and sustainable utilization of the geothermal reservoir.

The DAS monitoring system

On-site infrastructure and data acquisition

Schäftlarnstraße geothermal site

Geothermal energy has a fundamental role to play in the heat supply of the city of Munich (Germany). By 2040, 100% of the district heating network should be supplied by renewable energy (e.g. Farquharson et al., 2016; Cröniger et al. 2022). As part of this ambition, Stadtwerke München GmbH (SWM) developed in Munich, in Schäftlarnstraße (SLS), one of the largest inner-city geothermal fields in continental Europe to date, to cover the heating needs of 80.000 citizens. Hence, from the end of April 2018 to the end of May 2020, three pairs of injection and production wells were drilled and tested. All wells are deviated and reach the geothermal water-bearing carbonate formation of the Upper Jurassic period—the Malm—at about 2500 m below sea level (Schulz and Jobmann 1989; Böhm et al., 2013). In Fig. 1 (a), the trajectories of the production and injection wells (red and blue lines, respectively) are projected on the map of the Munich city center. Fig 1 (b) focuses on the well site and shows the well pad with the six wellheads, which are separated by about 8 m from each other. The wells follow a vertical trajectory at shallow depth and start to significantly deviate from about 800 m below surface.

On-site FOC equipment

Monitoring is a key component to ensure the sustainable exploitation of the geothermal resource. With this regard, fiber optic cables have been deployed at SLS in the TH3 and TH4 wells to evaluate the benefits of DOFS in such a context.

The coupling of the FOC to the surrounding medium plays a crucial role in DAS technology applications. At the SLS geothermal field, two different configurations have been considered for the TH3 and TH4 cables (Schölderle et al. 2021). In the TH3 injection well, the cable was fixed on the outside of the casing from surface to about 700 m, without any slack, and cemented (see Fig. 1 (c)). In the TH4 production well, the FOC is deployed from wellhead to total depth, using a sucker rod. Schölderle et al. (2021) propose a precise description of the cable settings and of the installation steps. Cemented cables do not interfere with well operations and generally provide tighter mechanical coupling to the surrounding, which is favorable for the acquisition of high-quality DAS data (Reinsch et al. 2013). On the contrary, Martuganova et al. (2021) report possible disturbing signals, originating from resonances at free hanging cable sections. However, cemented cables cannot be recovered or replaced and their installation must be done carefully to avoid any damage during run-in-hole and to ensure well integrity with an appropriate cementing job.

As the TH4 cable was not accessible during the study period, we focus here on acquisitions conducted solely with the TH3 cable. However, we discuss the extension of the concept to the joint use of both cables in Sect. "Outlook for a Reservoir Management System". Figure 1 (c) focuses on the completion of the injection well TH3. The section equipped with the FOC is considered as vertical, with an average deviation angle of 3°. One side of the cemented FOC is oriented towards the shallow geological layers of both the Quaternary and the Tertiary periods. The Tertiary layers, composed of clay, limestone and sandstone, are subdivided into several formations reflecting specific deposition conditions. In the stratigraphic column of Fig. 1 (c), "Obere Süßwasser Molass" (OSM) refers to sediments that were deposited in fresh water, "Süßbrackwasser Molasse" (SBM) describes sedimentation in a brackish sea and "Obere Meeresmolasse" (OMM) refers to sediments that were deposited under marine conditions. On the well side, the FOC faces a fluid-filled annulus, known as the tieback. The latter is positioned between the FOC and the inner well. The flow of reinjected geothermal fluid enters the Malm reservoir from the open-hole section, between 2571 and 3049 m TVD. In practice, the interrogated fiber provides redundant sensing of the vertical section due to the U-loop at 692 m. Figure 1 (d) shows the entry and exit points of the FOC at the TH3 wellhead (red square). Finally, both ends of the cable are accessible from the control room next to the well pad (gray polygon in Fig. 1 (b)).

DAS set-up for the test period

For the 6-months monitoring period, a Febus Optics A1-R recording system was connected to the sensing fiber in the control room for continuous acquisition of DAS. The interrogation unit is based on the phase-coherent optical time domain reflectometry (OTDR) technique. The principle consists in measuring the phase differences in the backscattered photons from neighboring positions along the fiber. This enables recording strain-rate (SR) over short distances called gauge-lengths (GL) and at several

positions along the fiber (see Juškaitis et al. (1994) for an experimental validation of the sensing technique). An extensive description of the possible DAS settings can be found in Masoudi and Newson (2016) and in Hartog et al. (2013).

To ensure optimal signal quality, the propagation velocity and frequency of the expected seismic waves should guide the selection of the DAS acquisition parameters. Among the latter, the GL is of particular importance. Insufficiently long GL degrade the signal to noise ratio, while excessively large ones may distort the shape of the observed wavelet. In this study, we set the signal sampling rate to 500 Hz and the GL to 10 m. Considering the apparent velocities observed in the study (between 1000 and 3500 m/s, see Sect. "Onset-time picking") and the frequency range used for detection (from 5 to 40 Hz), the ratio of apparent wavelength to GL should provide reliable assessment of the actual wavelength while minimizing the so-called gauge length effect (Dean et al., 2017). In conjunction with this GL, we used a 5 m spacing between successive measurements. The U-shape deployment of the FOC made it possible to decrease the spatial sampling from 5- to 2.5-m while processing the data, as described in Sect. "Data structuring".

Figure 1 (e) shows the installation in the control room, where the DAS interrogator is connected to an uninterrupted power supply (UPS). The UPS ensures the delivery of a stable alternating current to the equipment and prevents short power interruptions. All devices are stored and secured in a metallic shelter. Considering the location of the DAS interrogator relative to the well pad, the DAS recordings contain the signal acquired along the TH3 loop, but also from the control room to the TH3 wellhead. Hence, the portions of cable at surface and in the upper part of the well are particularly subject to disturbances arising from human activity, such as traffic of heavy vehicles or operations on the well pad. The same applies to the DAS interrogator installed in the control room. In Sect. "Data processing workflows", we further discuss the impact of the recording conditions on the data.

We conducted tap-tests at the TH3 wellhead in order to select the measurement points distributed along the well and assign them a physical location in terms of depth (TVD). Fig 1 (d) highlights the location where the FOC was repeatedly excited. These tests made it possible to identify which channels in the recorded datasets correspond to the ground level, both on the descending and ascending sections of the U-shaped fiber. This makes it possible to position the 0 m depth in the recordings accordingly, with an error of maximum half a spatial sampling distance (± 2.5 m). In addition, the depth corresponding to the lowest point of the cable was documented during installation (Schölderle et al., 2021). From both indications, we arrange the sensing points at 5-m intervals along the presumed straight (i.e. without slack) and vertical optical fiber.

Description of the cloud infrastructure

An inherent constraint of DAS is the possibly large amount of data it generates, which is particularly impactful in the context of continuous and permanent monitoring. In this regards, two scenarios may be envisaged. Acquisitions can be processed on site using local resources to limit the amount of data to be transferred, which is reduced to the analysis outcomes. Alternatively, the generated data flow can be transferred efficiently for remote processing. With the perspective to consider DAS as one seismic station among others and to integrate it in a larger seismic monitoring network, we selected the

second option and used a cloud infrastructure in view of the efficient processing of the DAS acquisitions.

Cloud computing services provide access to storage and processing resources that can meet operational requirements in terms of performance, scalability and level of access to the data. Their flexibility allows resources to be adapted to actual needs while allowing for possible upscaling, for instance to unify on a single platform the collection and processing of data from different DAS stations at different sites (as discussed in Sect. "Outlook for a Reservoir Management System"). A remote and secured access to the DAS data for the operator and stakeholders can also be implemented. Finally, operators may already rely on such services (see below).

Therefore, a procedure was implemented to store and process DAS data leveraging cloud services used by the geothermal field operator (see Fig. 2). With the acquisition parameters described in Sect. "DAS set-up for the test period" 1.4 MB are generated every second by the DAS interrogator and buffered in Hierarchical Data Format 5 (HDF5) binary files. The DAS files were written on the solid-state drive (SSD) of the interrogator, which behaves as a fast and efficient buffer. Besides, the interrogator was connected to the second component of the monitoring system, the cloud platform designed to manage the data.

The cloud application platform

Figure 2 (a) illustrates the monitoring and data management system. The system links the onsite infrastructure (i.e. well pad and control room devices) to the Internet of Things (IoT) cloud platform developed to host specific archiving and processing modules. The setup ensures an efficient and secure data flow via the company's intranet and

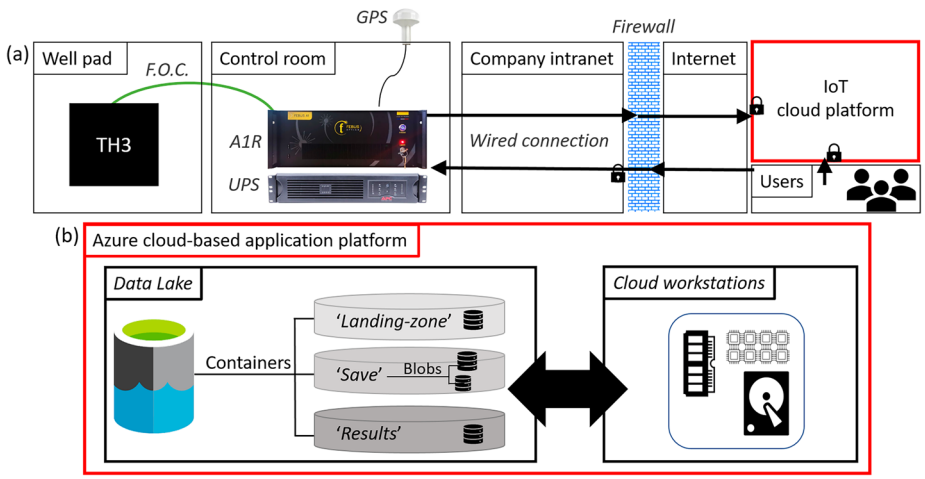

Fig. 2 Panel (**a**) schematic view of the monitoring system proposed to link the TH3 FOC, the Febus A1-R interrogator, the developed IoT cloud platform and the users or developers of the infrastructure. The locks are meant to highlight a secured connection. Panel (**b**) focus on the conceptual structure of the IoT cloud platform developed to connect the Febus A1-R interrogator to a cloud application platform based, here, on Microsoft's proprietary solution, Azure Cloud. It is subdivided into two entities able to communicate through standardized data exchange. The so-called "data lake" constitutes the data storage environment, which is organized into "Containers" and "Blobs". The associated structure is comparable to the more common-known directory and file system. Cloud workstations are used to process the datasets using scalable resources

enables a hierarchical remote connection of the users to both the interrogator and the cloud platform.

The IoT cloud platform is described in more detail in Fig. 2 (b). It has been developed using Azure, the cloud application platform of Microsoft, which bundles a set of public IaaS (Infrastructure as a Service) and PaaS (Platform as a Service) services. A detailed review of the services available from Azure is to be found in Soh et al. (2020a, 2020b). The choice of this specific cloud-service provider was motivated by the fact that the field operator, SWM, uses it to monitor the heating plants and networks they have in charge in the Munich region. Thus, it was intended to assess whether the system in place could be used to develop a DAS monitoring component. Additionally, this offers perspectives to link different monitoring aspects within the same cloud infrastructure. In our case, associating seismic and geothermal field operation monitoring would be of particular interest to implement a sustainable reservoir management system, as discussed in Sect. "Outlook for a Reservoir Management System".

While the following description of the IoT cloud platform refers to services provided by Microsoft Azure, the concept can be transposed to any other competing cloud platform or service provider, as long as they feature similar storage resources and processing capabilities. The adaptability of the concept is also demonstrated through the utilization of Python-coded scripts for the handling and management of the data flow (see Sect. "Data processing workflows"). A comparative analysis of environments provided by major cloud service providers, namely Amazon, Microsoft and Google, can be found in Dzulhikam and Rana (2022), for instance.

Technically speaking, two interconnected Azure services, namely Azure Data Lake Storage and Azure ML Studio, are used on the IoT cloud platform to fulfil the data archiving and processing tasks, respectively. These services meet the data management system's requirements in terms of amount of stored data, level of access and efficiency of IT processing.

Data storage solution

The generated DAS binary files are stored on a so-called data lake [left hand-side of Fig. 2 (b)]. This storage environment offers a scalable and hierarchical file system. It is based on a proprietary solution dedicated to storing objects in the cloud called Azure Blob. The latter is optimized for storing large amounts of unstructured data, such as textual or binary data.

Fig. 2 (b) also focuses on the structure of the data lake. The sketch emphasizes the three types of resources available to the user to organize storage environments. The data lake can be subdivided into so-called containers, which themselves include the blobs, i.e. the stored items. The latter is associated here to individual DAS data files generated by the interrogator, or results from the data processing.

An important aspect of the storage solution is the access-right management. The management of this storage environment is assigned to a user account. The use of Shared Access Signature (SAS) tokens ensures secured and delegated access to the resources. Every resource is therefore assigned a unique address making it possible to grant user-customized access permissions. The three previously mentioned structures (i.e. account,

containers and blobs) can be respectively compared to file systems, folders and files, which are more familiar objects in IT.

Another key feature of the storage solution is the ability to manage the associated costs. It involves organizing the saved data according to the frequency of access and storage duration by assigning specific access levels. Typically, the access level for infrequently used data is applied to the resources stored in the "*Save*" container [see Fig. 2 (b)], which are full DAS data files saved after processing. This tier provides lower storage costs but larger latency and delays in the data access. The same applies for the resources of the "*Result*" container, which archives the elements resulting from the data processing, i.e. approximately 1 MB per detected event. Hence, the properties of the data storage environment allowed all the produced resources to be stored seamlessly, including the entire 6-month time series of DAS data (4122 files representing a total amount of about 21 TB). On the contrary, the resources stored in the "*Landing Zone*", i.e. the environment containing files awaiting processing, are assigned an access level that is designed to achieve high performances in reading and exchanging data.

Data processing solution

Cloud-based workstations [right side of Fig. 2 (b)] provide the computational resources needed to process the flow of data reaching the storage environment. These workstations are available from an online workspace allowing users to develop, run and automate the launch of notebook-based scripts.

A key aspect of these workstations is their scalability to user-defined needs. Thus, the properties of the available hardware is optimized in terms of memory capacity, number of physical or logical cores and local storage volume. Furthermore, additional specific tools and libraries can be installed on the system. Finally, the cloud workstations have the advantage of providing direct access to the computational resources being queried. This feature avoids the queuing system typically associated with High Performance Computing (HPC) clusters.

In our case, the cloud workstations have been scaled to sustain significant memory and CPU-to-memory loads, to enable large DAS files to be efficiently loaded in the Random Access Memory (RAM). Additionally, Python-based codes suitable for seismic processing and the underlying Obspy library (Beyreuther et al. 2010) were imported and installed.

Data processing workflows

The cloud-based processing of the acquired DAS data aims at providing a catalogue of possible induced seismicity with the associated waveforms. The Python scripts running on the cloud-based workstations are intended to read and structure the DAS data files landing in the storage environment in the form of blobs and apply the seismological processing workflow.

Data structuring

The reading of the DAS acquisitions of the "*Landing Zone*" is done from the cloud-workstations using the Python client package dedicated to the reading of blobs, i.e. the stored items. The duration of a stored items can be adjusted to the needs, e.g. to tend towards

real-time monitoring (see Sect. "Towards real-time seismic monitoring of geothermal fields"). Secure access is provided by the SAS tokens assigned to the container. Once the strain-rate data of a given blob is loaded into the RAM of the cloud-workstation, we extract the measurement points along the TH3 well. These points were identified using tap-tests, which determined the nearest entry and exit points in TH3 (see Sect. "DAS set-up for the test period"). Then, the depth of each measurement point is assigned based on a regular 5-m spatial sampling, under the assumption that the U-turn located at a depth of 692 m has no bending radius. Since the interrogated optical fiber has downward and upward segments in TH3, it results in an effective depth sampling along the well smaller than 5 m. We use this spatial redundancy to reduce the spatial sampling from 5 to 2.5 m. This is done by repositioning the upward measurement points onto a uniform grid, using a linear interpolation between the adjacent traces. As a result, the analyzed DAS datasets contain 280 traces with the associated measurement points covering the initial 692 m of TH3. To account for seismic events that may overlap successive files, 2D datasets are systematically merged with the last 10 s of the preceding files. The resulting dataset is finally structured as an Obspy stream (Beyreuther et al., 2010), with a spatial and temporal sampling of 2.5 m and 2.0 ms, respectively. Then it enters the seismological processing workflow that features data de-noising and event detection.

Data de-noising

Compared to conventional seismometers, recordings obtained using DAS systems generally exhibit higher noise levels (e.g. Correa et al., 2017; Olofsson and Martinez, 2017). The causes of these disturbances may be multiple and their impact on the recordings can vary along the cable. Lindsey et al. (2020) review several factors influencing the quality of the DAS data, from the interrogator and fiber environment to the sensing method itself. Therefore, DAS recordings have been subject to various developments in de-noising methods. While one dimensional time-frequency Butterworth filters are effective in suppressing noise in a given frequency band, the dense spatial sampling achieved with DAS and the spatial coherence of the observed wavefields allow the application of various 2D de-noising approaches, which are inherited from array processing and active seismic experiments. Among those, filtering in the frequency-wavenumber (*f-k*) domain (Duncan and Beresford, 1994) can be applied to suppress the energy associated with identified disturbances or incoherent noise, which may result in an enhancement of the signal-to-noise ratio (Isken et al., 2022).

For event detection, we bandpass filter the strain-rate acquisitions in the 5 to 40 Hz frequency band, which corresponds to a typical frequency range for the detection of local induced seismicity (e.g. Maurer et al., 2020). However, as noted in the Sect. "On-site infrastructure and data acquisition", the geothermal field activity has a strong impact on DAS recordings in the target frequency band. Figure 3 (a) illustrates the two main types of anthropogenic disturbances observed in the DAS recordings of TH3.

First, the DAS interrogator may vibrate in its rack, which leads to the recording of high amplitude signals, which are overprinted on all traces. These spiky signals are attributed to laser-noise (Zhirnov et al., 2019) and can lead to spurious detections. Secondly, surface activity occurring close to the well may generate acoustic waves propagating in the fluid within the tieback of TH3 [see Fig. 1 (c)]. These

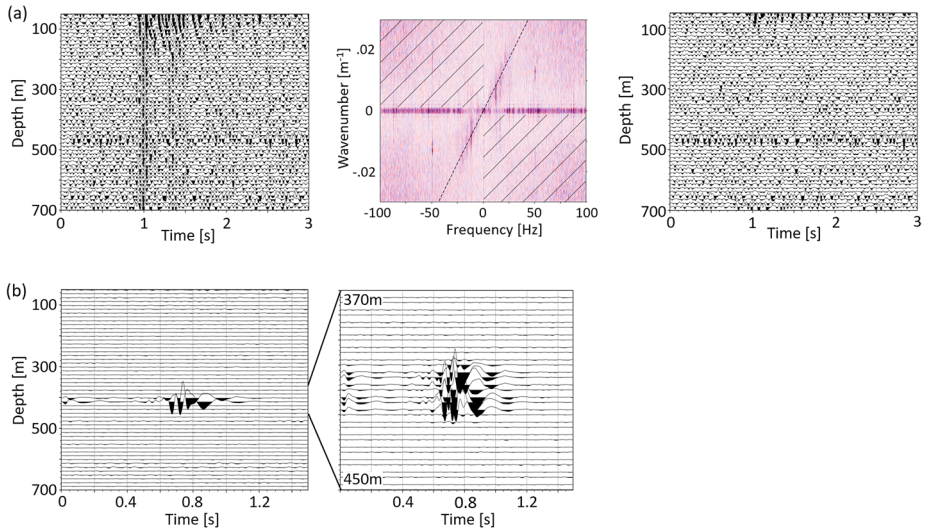

Fig. 3 Overview of different types of noise recorded in the target frequency band. For visual and illustrative reasons, the dataset is first filtered below 100 Hz. Panel (**a**) illustrates the impact of the surface activity associated with the operation of the geothermal field where the acquisitions are conducted. From left to right, the dataset is shown in the time-depth domain, then in the frequency-wavenumber (f-k) domain and, finally, back into the time-depth domain once filtered in the f-k domain. The f-k filtering consists in keeping the hatched areas (middle figure) and suppressing the energy related to known noise sources. The dashed line highlights the signature of a down-going wave propagating from the surface along the well at 1500 m/s. Panel (**b**) shows, in the time-depth domain, a strong local signal related to workover in one of the wells near to TH3

acoustic waves may eventually be transmitted to the fiber, resulting in the observation of down-going waves propagating at approximately 1500 m/s. Consequently, to avoid numerous false detections, the datasets are additionally filtered in the *f-k* domain. Our approach consists in keeping the energy of the waves propagating from the lowest part of the fiber towards the surface. This is justified by the fact that potential local seismic events should originate from depths larger than 692 m. The middle panel of Fig. 3 (a) shows the signature of the previously described noise in the *f-k* domain. It shows the propagation of waves along the entire fiber at an infinite velocity, visible on the horizontal axis of the *f-k* domain. It also depicts waves propagating at increasing depths at velocities typical of acoustic waves in fluids, leading to high energy components in the domain with positive wavenumbers and positive frequencies (or vice-versa, i.e. top-right or bottom-left quarter). One can also observe a strong 50 Hz component, which is typical of noise induced by the alternating current of the electrical grid. Thus, the filtering consists in isolating the domain associated with positive wavenumbers and frequencies, or vice-versa (i.e. the hatched part of the *f-k* domain). As shown on the right panel of Fig. 3 (a), the proposed approach successfully removes the previously identified waves.

Additional strong noise, which impact the dataset locally, i.e. on a short depth range, cannot be filtered by the proposed processing. Figure 3 (b) shows how completion operations, typically here the installation of an electric submersible pump in a well near TH3, can affect the DAS recording. This interference is explained by the small distance between two adjacent wells along their vertical part, down to ~ 800 m

(TVD), the wellheads being separated by about 8 m on the well pad. However, these types of local noise will not result in spurious detection with the event detection workflow described below.

Event detection

Once properly structured and filtered, the dataset enters the detection workflow. The objective of the proposed DAS monitoring is to detect microseismic events potentially induced locally, i.e. within a 5 km radius, during reservoir exploitation. Our approach is based on the recursive STA/LTA algorithm (Withers et al. 1998; Trnkoczy 2012) implemented in the Obspy library (Beyreuther et al. 2010). The detection parameters are detailed in Tab. 1:

In order to use the multiple DAS channels jointly and compensate for possible noisy channels, we use the computed coincidence sum as detection metric. With this approach, which is commonly applied with large networks of sensors, all single station triggers are combined to identify possible time overlaps that will be interpreted as a synchronous event. Hence, the coincidence sum gives the number of individual overlapping triggers (Withers et al. 1998; Trnkoczy 2012). Here, a detection occurs when the coincidence sum exceeds 30 traces (see Tab. 1), which is equivalent to a 70 m long section of adjacent triggers. Nevertheless, no constraint has been provided regarding the clustering of the single triggers over depth.

Once a DAS dataset is processed, the detection report (i.e. list of triggers, including detection time, triggered traces, etc.) is appended and saved in the "*Results*" container with the corresponding waveforms, i.e. 6-s long data subsets, unfiltered, centered on each detection and written in mini-SEED format. The processing workflow was initially tested using hourly-generated DAS-files. On average, the full processing of one of these 5.04 GB large files took 11 min with 8 processors (2.7 GHz Intel Xeon® Platinum 8168) on the cloud workstation, without distribution nor parallelization of the tasks. The extension of this approach to real-time monitoring is discussed in Sect. "Discussion".

The detection results are occasionally downloaded locally for quality control and post-processing, which includes the picking of the seismic phases. The results of the post-processing of two microseismic events are presented in Sect. "Monitoring results".

Monitoring results

During the survey, 4122 files were acquired, saved and processed following the described procedure. Over the 6-months period, the DAS interrogator recorded continuously except for short periods during which the GPS signal was lost. This section presents the results obtained in terms of detections and dataset characterization.

Table 1 Event detection parameters based on a recursive STA/LTA and a coincidence sum

Trigger activation (STA/LTA ratio)	Trigger off (STA/LTA ratio)	Short-time average (STA)	Long-time average (LTA)	Coincidence sum
2.3	1.3	0.3 s	3 s	30

Spectral content of the DAS recordings

As an initial evaluation of the collected DAS data, we analyze the frequency content using probabilistic power spectral densities (or PPSD, see e.g. McNamara (2004)). PPSD are commonly used to statistically evaluate noise levels at different frequencies. To obtain noise levels representative of the day and night fluctuations, we analyze 48 h of the collected strain-rate data. At each sensor, the PPSD is computed from 192 data segments of 30 min. Figure 4 (a) shows the median across individual frequencies for the PPSD computed at each measurement point along the TH3 optical fiber. The dashed lines delimit the frequency band used for event detection, i.e. from 5 to 40 Hz.

Figure 4 (b) focuses on the evolution with depth of the spectral energy between 5 and 40 Hz (black curve) and highlights the influence of the anthropogenic noise on the shallow section. Between surface and 50 m, the noise spectral energy decreases by a factor of two. Deeper than 50 m, the curve shows that the average noise level does not significantly decrease with depth. Figure 4 (c) focuses on the lowest frequencies of the shown spectra, below 0.1 Hz. In both frequency bands, the noise profiles (below 50 m) look relatively similar, except at specific depth, e.g. around 600 m. In both cases, comparable noise fluctuations exist over depth, some of them covering the whole frequency range, e.g. at 330 m or 390 m (Fig. 4 (a)). To investigate the origin of the observed variations, the average DAS spectral energies (black curves) are compared with the Cement Bond Log

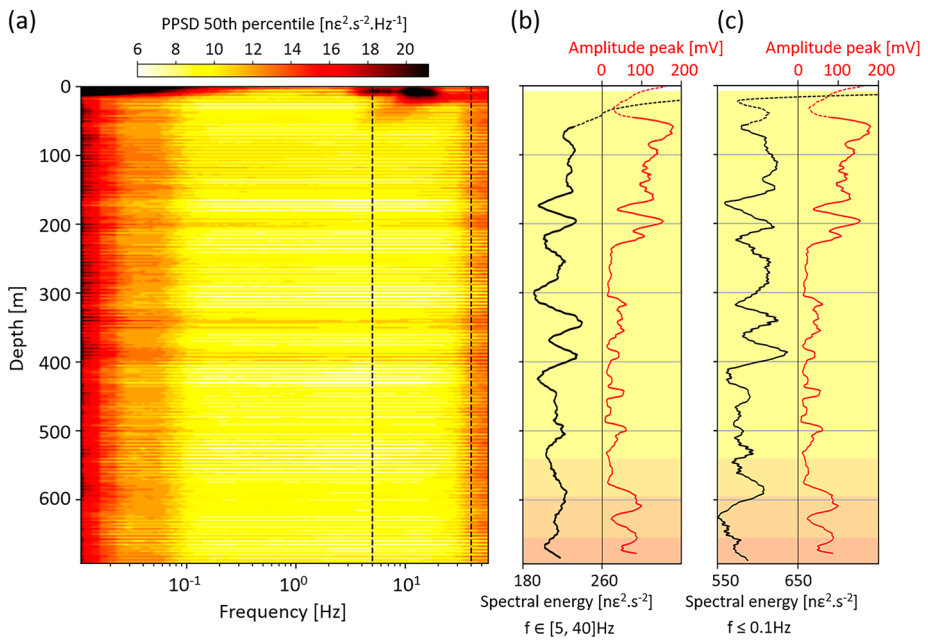

Fig. 4 Spectral content of the DAS recordings at the study site. Panel **a**: Evolution with depth of the frequency content of the strain-rate data acquired on two consecutive days. The probabilistic power spectral density (PPSD) is computed from each time-series, using 192 data segments of 30 min. The color scale indicates the median PPSD at the sensor depth. The frequency band from 5 to 40 Hz is bounded by the dashed lines. Panel **b** Evolution with depth of the spectral energy (the integral of the PPSD) in the 5–40 Hz frequency range (black curve and bottom black abscissa) in parallel with the amplitude of TH3 cement bond log (CBL) (red curve and top red abscissa). The colored background represents the lithological units defined in Fig. 1 (**c**). The spectral energy curve and the CBL amplitude have been filtered with a moving average filter of 10 m. Panel **c**: Same as panel **b**, but considering the energy below 0.1 Hz (black curve)

(CBL) acquired in TH3 in December 2019 (red curves) and the lithological units. CBL are generally used to check the casing cementation job, which constitutes one aspect of the well integrity monitoring. Amplitudes of CBL are smaller with a good cement bond than with a partial bond, or no bond at all (free pipe) (e.g. Pickett, 1963). The similarities observed between the DAS spectral energy profiles and CBL below 50 m, especially around 200 and 600 m, are further discussed in Sect. "Monitoring capabilities of DAS along well".

Fig. 8 provides additional insight into the temporal variations of the spectral content of the DAS recordings. It illustrates the temporal and depth-related changes in the average spectral energy within the 5 to 40 Hz frequency range. The figure is based on individual power spectral densities (PSD), which are computing at each measurement point using 30-min long recordings. The time-period represented in Fig. 8 covers one working week, from Monday to Sunday. It highlights the daily and weekly variations of the spectral energy. This background noise level correlates well with the anthropogenic activity that affects the first 40 m of fiber during the working hours, in agreement with Fig. 4. The figure also shows that the continuous operation of the geothermal field influences permanently all sensing depths from surface down to 20 m, regardless of working hours.

Local seismic event analysis

Seismic event detection

To evaluate the capability of DAS to detect local induced seismicity from the flowing TH3 injection well, we compare the seismic catalog obtained from the 6-month DAS monitoring with the one obtained from the nearby seismometers.

During the monitoring period, several regional and two local seismic events were detected with the proposed DAS monitoring system. We focus in this paragraph on these two detected local seismic events. The status of the seismometer network operating near the SLS site is described e.g. by Azzola et al. (2021, 2022). These seismometers, including the two stations situated close to the SLS site [see Fig. 1 (a)], are used to evaluate this catalog. These local events are not listed in the catalogue of the Bavarian seismological services and no other event is listed in this catalogue during the DAS monitoring period near the site. The first one, of local magnitude M_L 1.5, occurred on February 9, 2022. The event was recorded by the surface seismic stations located in a radius of 10.4 km and located at a distance of about 10 km to the TH3 wellhead, originating from the Malm layers. The second one occurred on April 22, 2022. Other than in the DAS measurements presented here, it was vaguely identifiable on only one other 3C-seismometer, which is deployed in a well located approximately 1 km east of the TH3 wellhead (T. Megies–LMU, personal communication). It was not visible on any other seismic station in the vicinity. Its characteristics have not been evaluated yet.

Figure 5 highlights the ability of DAS in TH3 to detect the April 22 event, solely triggered by the DAS monitoring system. For every measurement point along TH3, we show the characteristic functions of the recursive STA/LTA algorithm (Fig. 5 (a)), with red and blue dots indicating the activation and deactivation of the trigger, respectively. The characteristic functions illustrate the possibility to trigger simultaneously P- and S-waves. We also analyze the evolution with depth of the maximum STA/LTA ratio measured along the characteristic functions (Fig. 5 (b)). The curve shows significant variations in

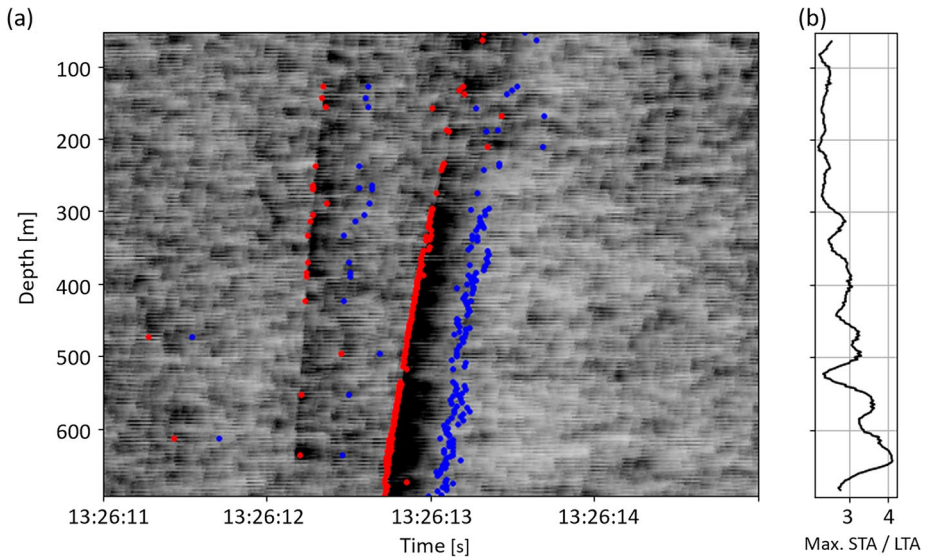

Fig. 5 Characterization of the detection sensitivity level of the April event. Panel (**a**): Characteristic functions of the recursive STA/LTA algorithm, which was applied to each strain-rate time-series. Red and blue dots show the coordinates at which the trigger turns on and off, respectively, with the parameters in Tabel 1. Panel (**b**) Evolution with depth of the maximum STA/LTA ratio measured along the characteristic functions presented in panel (**a**)

the ratio within the investigated depths. These variations are further examined in Sect. "Monitoring capabilities of DAS along well" while discussing the monitoring capabilities of DAS, in view of the background noise conditions.

Figure 6 shows the bandpass- and *f-k* filtered strain-rate data associated with the February (panel a) and April (panel b) events. The bandpass-filtered datasets are additionally shown in Fig. 9 to highlight the improvements in signal-to-noise ratio and signal coherence achieved by the de-noising strategy in the f-k domain. The left panels of Fig. 6 give an overview of the multiple arrivals that can be identified along the 692-m DAS recordings. The middle and right panels focus on the first P- and the first S-waves, respectively. Both wave types are clearly discriminated using their apparent velocities along the fiber, which is larger for the P-wave than for the S-wave. Interestingly, one can also observe that the S-waves maximal amplitudes are larger than for the observed P-waves. The figure also highlights the distinctive characteristics of both events. In Fig. 6 (a), i.e. for the February event, successive scattered P- and S-waves can be observed in the 3-s data-window, and the first S-wave is dominant at a frequency of 8 Hz, lower than the P-wave frequency, around 25 Hz. The higher frequency content of the April event captured in Fig. 6 (b), the lower delay between the P- and S- waves, and the lack of multiple scattered waves are characteristics of a nearby event. This shows that the insensitivity of the TH3 fiber to horizontally incident waves is not a major constraint to properly identify onset times of local events.

Onset-time picking

In view of extending the processing workflow to event characterization, we picked onset-times for both local events. The depth variations of P- and S-wave arrival times are shown in Fig. 6 (see continuous black curves). The onset-times were obtained

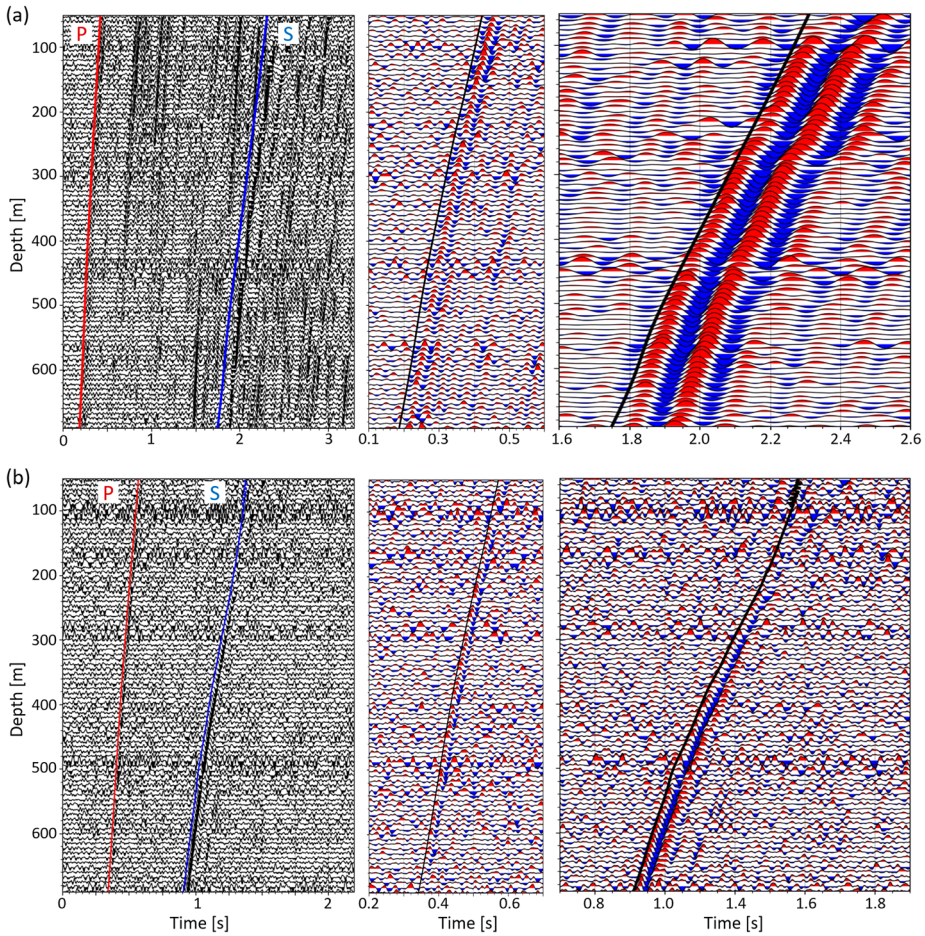

Fig. 6 Strain-rate of the local February (panel a) and April (panel b) seismic events detected on the entire interrogated fiber. The left panels show the multiple arrivals including the first P- and S-waves. The middle and right panels focus on the first P- and first S-arrivals, respectively. The curves on the waveforms indicate the results of the semi-automated first arrival picking. Panel (**a**): the February event is located about 10 km away from the SLS geothermal site and has a magnitude of M_L 1.5. The horizontal axis indicates seconds after 2022.02.09 05:51:30.7 (UTC). Panel (**b**): April event. The horizontal axis shows seconds after 2022.04.22 13:26:11.8 (UTC)

trace-by-trace using a semi-automated picking algorithm applied—for the time-being—outside the cloud and available in the Reveal© software (Shearwater) dedicated to active seismic data processing. To identify the wave arrival within the background noise, the algorithm requires reference picks and the size of the search window defined around these reference measurements. The process is not fully automated, as the user must specify at least three reference measurements, later propagated to all other traces. The algorithm necessitates the additional definition of the size of the window used to compute the baseline signal level. The initial break time (zero crossing) is then determined independently for each trace from the baseline amplitude estimated prior to the reference picks.

Figure 6 shows that the first P-wave arrivals have been consistently identified over the entire fiber for both events. Nevertheless, although the automatic picking for the S-wave is correct along most of the fiber, this is not true for its shallowest, nor its deepest part.

For the first 100 m (respectively 200 m) associated with the April (February) event, the origin is likely the larger background noise evidenced at these depths, which is not totally discarded by the applied filtering. For the February event, which is the stronger of the two studied, the interference between the S-wave and the multiple P-waves adds to the effect of surface activity.

Preliminary event and site characterization

A precise location and characterization of both local events from the DAS data will be the focus of future work. However, Wadati diagrams (Wadati and Oki, 1933) were computed for preliminary characterization using the most reliably picked P- and S-arrivals, i.e. for depth larger than 100 m (see previous paragraph). The corresponding Wadati diagrams are presented in Fig. 10. Approaches based on Wadati diagrams have their limitations, especially as the Vp/Vs ratio is assumed the same in all media along the raypath (Wadati and Oki, 1933). However, the diagram provides a first estimate of the April 22 origin time, which compensates for the lack of any other seismic observations. Thus, the estimated origin time is 2022–04-22 13:26:11.77 (UTC) with an uncertainty of ± 0.02 s when accounting for the seismic wave period. Using the estimated origin time, the P-wave arrival times at each sensing depth and a homogeneous P-wave velocity, it is possible to estimate the depth and horizontal offset of the event from the vertical array of DAS measurement points. We use here an average P-wave velocity of 3000 m/s, which gives a hypocenter at a depth of 1700 m TVD (1180 m below sea level) with a horizontal offset of 500 m from the DAS antenna. Hence, this April event likely has its origin in the Tertiary sedimentary cover, rather than in the geothermal reservoir (the Malm carbonate formation). A refined hypocenter and origin-time inversion, using a more detailed velocity structure, will be the focus of posterior analysis.

The Wadati diagrams also provide information for site characterization. Here, we use the measurement to analyze changes in the apparent P- to S-wave velocity ratio (VP/VS) along the fiber. Figure 10 highlights two distinct trends, with an inflection point at approximately 500 m, at the end of the so-called "Obere Süßwasser Molass" formation (OSM). The calculated apparent VP/VS ratios are 2.5 and 2.2 for the surface and deep parts, respectively.

For both events, the variation in depth of the P- and S-wave arrival times allows us to characterize the changes along the FOC in the apparent velocity of the seismic phases. This apparent velocity is dependent on the incidence angle of the considered wave (at the FOC) and the associated propagation velocity at that depth. Thus, a change of apparent velocity may be attributed to a change of local velocity and associated incidence angle. The result is illustrated in Fig. 7. Each apparent velocity profile is computed by differentiating the associated arrival time profile and by applying a moving average filter of 10 m. For both events, we observe a significant increase in velocity near the interface between the OSM and SBM (layer "2" and "3" in Fig. 7). A sharp change in slope is initiated for both P-wave curves at the same interface. The location of the change is consistent with the position of the inflexion point in the Wadati diagrams, discussed earlier in this section. This result can provide valuable insights into the positioning of interfaces within velocity models. All profiles also highlight notable changes inside the thick OSM formation, which is mainly composed

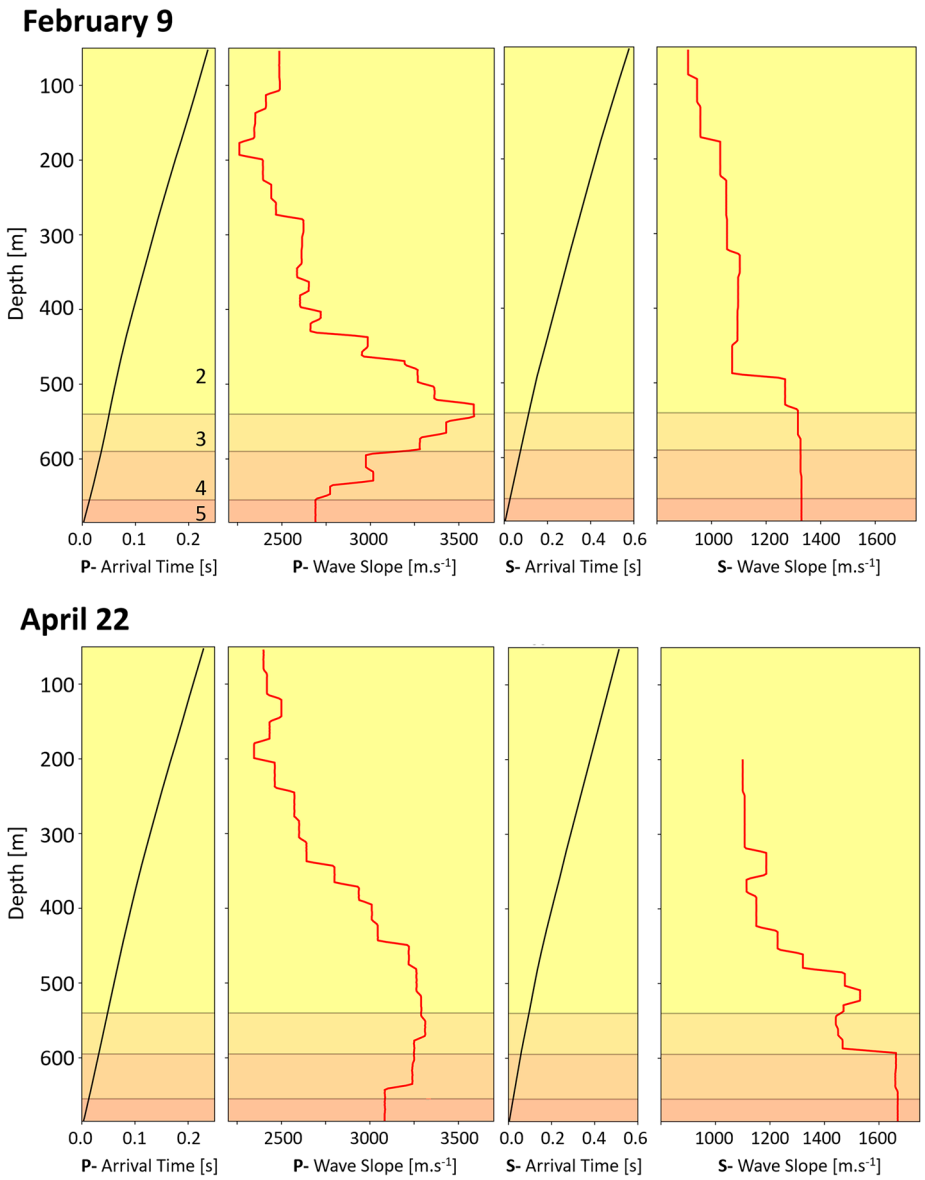

Fig. 7 P- and S-wave arrival times (left panels, black curve) and slopes (right panels, red curve) for the February (top) and the April (bottom) events. A moving average filter, whose period corresponds to the GL, i.e. 10 m, is applied on the raw profile before plotting. The background color shows the lithological changes and the numbers of the top-left panel refer to the column presented in Fig. 1 (**c**)

of clay marl, sand and gravel layers. The apparent velocity changes observed may indicate variations of the geomechanical properties and outline the inhomogeneity of the formation.

In terms of absolute amplitudes, the two profiles calculated for S-waves show a difference of 300 m/s at their maximum. However, absolute velocities must be carefully compared from one event to the other. Indeed, Fig. 7 focuses on apparent velocities measured along the vertical FOC. The February event originates from the Malm reservoir, several kilometers away from TH3, while the April event occurred much closer and shallower. Considering the location of both events, the P- and S-waves will intersect

the FOC with distinct incidence angles, which subsequently affects the amplitude of the analyzed velocity component.

Discussion

In light of the results of the 6-month continuous monitoring period, we now evaluate the usability of DAS in the routine operation of the geothermal field.

Monitoring capabilities of DAS along well

The results presented in Sect. "Monitoring results" support that DAS in well(s) advantageously complements standard monitoring approaches of geothermal fields from surface (e.g. Arbeitsgruppe „Induzierte Seismizität " des FKPE e.V., 2012). For both events, the P- and S-phases could be identified, which proves the capacity of DAS to consolidate the recordings delivered by three-component seismometers and opens promising perspectives in terms of localization and characterization of seismic events. Lior et al. (2021) showed in particular the ability of DAS-based approaches to resolve source parameters using P-waves on horizontal ocean-bottom fibers. With regard to the SLS site, the utilization of DAS waveforms for the further characterization of seismic events is currently investigated. In addition, the level of detection achieved for the April event demonstrates the capability of the technology to monitor a geothermal field in an urban area from a flowing injection well. The cemented FOC acts effectively as a long linear array of sensors positioned in closer proximity to the monitoring target, enabling the detection of low magnitude events that surface seismometers might otherwise fail to identify. The recursive STA/LTA characteristic functions (Fig. 5) provide indications of favorable signal-to-noise ratios, despite the influence of surface noise and the apparent low magnitude of the event (Sect. "Seismic event detection"). Fig. 5 (b) shows in particular that the STA/LTA ratio of the S-wave is larger than three in the deepest part of the FOC, which satisfies the FKPE criterion on the SNR required for reliable identification of a seismic wave (Arbeitsgruppe „Induzierte Seismizität " des FKPE e.V., 2012). In the future, more sophisticated detection methods can be explored to leverage the capabilities of the dense array of sensing points. This includes template matching techniques (Li et al., 2018) or approaches that benefit from the strong data coherency within the recording array (Lellouch et al., 2019). Nevertheless, their implementation on cloud workstations will depend on a prior assessment of the impact on processing durations and on the detection improvement.

Interestingly, Fig. 5 (b) shows notable variations in the maximum STA/LTA ratio along the optical fiber. This variability indicates that the capabilities of the method to trigger events changes with depth. The trigger method relies on measurements of the average signal envelope and its effectiveness at depth, for fixed working parameters (see Tab. 1), depends on local recording conditions. By comparing Fig. 4 and Fig. 5, we observe that lower STA/LTA ratios can be associated with increased noise levels in the DAS data (e.g. around 200 and 600 m). In Fig. 4, we additionally investigate whether this variability can be linked to alterations in cement bond quality and their effect on fiber coupling conditions. Prior studies already established a correlation between downhole DAS data and a cement-bond-log (CBL). Raab et al. (2019) showed that variations and patterns in a CBL align with the average strain-rate DAS data acquired from behind casing. Furthermore,

previous studies indicated that low-frequency DAS data provide additional insight into the well and its surroundings [e.g. Haavik 2023; Jin and Roy 2017). We investigate these aspects in well TH3 by looking at the average spectral energy in the frequency band used for detection (Fig. 4 (b) and below 0.1 Hz (Fig. 4 (c)]. At shallow depth, we notice a significant impact of surface noise on the recorded DAS energy (shallower than 50 m). The DAS and CBL curves present similarities, especially around 200 and 600 m. These similarities are particularly noticeable below 0.1 Hz, notably around 600 m (Fig. 4 (c). This observation suggests that a poorer cement bond would lead to a weaker coupling of the fiber with the formation and result in higher noise levels on the DAS and reduced sensitivity of the detection method. From an operational point of view, the correlation between DAS background noise and CBL suggests the potential for continuous monitoring of well cementation using DAS data. Nevertheless, we do not demonstrate a uniform alignment between STA/LTA ratios, spectral energy profiles, and the CBL along the entire fiber. In particular, the peak in spectral energy observed around 400 m is associated with a good CBL and steady STA/LTA ratios. Potential explanations for this discrepancy include the directional nature of the CBL measurement, which might overlook azimuthal variations in cement quality or channeling effects. Additionally, recording conditions at depth might be influenced by factors other than the quality of coupling. This applies to the studied configuration, where the eight wells are close to each other and their operation (fluid circulation or maintenance) can influence the measurements at depth (see Sect. "Data de-noising"). In addition, Li et al (2022) demonstrated an apparent correlation between major noise RMS amplitude peaks and anomalies in conventional logging data associated with low-velocity layers bounded by sharp structural interfaces. This study also suggests a potential link between DAS noise levels and the surrounding geology.

Finally, the aforementioned monitoring capabilities can be compared to those of a string of geophones. Assuming a FOC and a string of 3C-geophones were installed alongside each other with comparable coupling conditions, geophones would likely demonstrate superior absolute detection sensitivity compared to DAS, primarily due to the influence of optical and self-induced noise (Lindsey et al., 2020). Nonetheless, when considering the practical context of operational deployment, installing and cementing a 3C-geophone string raises important concerns regarding the overall well integrity. Due to its slimmer and robust construction, the FOC presents a significantly reduced risk in this aspect. In contrast, DAS prevents locating an event using a single monitoring well due to the unidirectional measurement it provides. The configuration investigated here at the SLS site, featuring a single vertical FOC, allows inverting the depth and offset of the seismic source with respect to the DAS antenna, but additional data are required to resolve the back azimuth. Hence, unless several sites or wells would be instrumented, DAS needs to be complemented by other equipment (e.g. surface seismometers) to be able to reach seismic monitoring objectives (e.g. location capabilities), but possibly at the cost of a higher magnitude of completeness. Nevertheless, the installation of FOC in geothermal wells enables the utilization of a single sensing element to monitor various physical parameters. A FOC is usually made of several single and multi-mode fibers that can be used for a variety of applications. This potential, which is further discussed in Sect. "Outlook for a Reservoir Management System". has been evidenced and leveraged

by the oil and gas industry for at least one decade (Koelman et al., 2012; Koelman 2011; Van Der Horst et al., 2013).

Towards real-time seismic monitoring of geothermal fields

The use of DAS for monitoring geothermal field operations requires a degree of sensitivity in detecting events, which has been discussed in Sect. "Monitoring capabilities of DAS along well". For hazard mitigation purposes, the monitoring system must also provide the results, i.e. seismic activity catalogues, as fast as possible. Therefore, incorporating a DAS system into the monitoring strategy of the geothermal field calls for an efficient transfer of large amounts of data and their optimized processing. These requirements were met with the cloud platform used as a unified service that combined storage, accessibility and data processing (see Sect. "Description of the cloud infrastructure"). To assess the capabilities of the concept to tend towards real-time data processing, we processed 1-min long DAS recordings. According to the workflow described in Sect. "Data processing workflows", this task took on average between 9 and 10 s for each file, which is at least six times faster than the file duration and thus avoids the occurrence of overflows. The transfer of the data to the storage environment also influences the delay between the event occurrence and its actual detection. With the observed uploading rate of 36 MB/s, less than three seconds were necessary to upload one-minute-long files from the interrogator to the Data Lake. Consequently, the full handling of 1-min long DAS recordings allowed to deliver automatic detection results with a delay of at most 1 min 13 s after a possible event onset time, which shows great potential for real-time monitoring.

To tend further towards real-time processing of the acquired datasets, different improvements can be considered:

- Under its current operating conditions, the interrogator needs to write a full HDF5 file on the SSD before pushing it towards the Data Lake. The option to stream on a real-time basis the data, as it can be configured on the present seismological digital recorders, would decrease the delay between a recorded DAS signal and the associated results, thus suppress the limitation associated with the file buffering on the interrogator.
- The band-pass of the wired connection used to transfer the data could be decreased. However, this limitation is much less restrictive than the current file buffering and the uploading rate easily absorbs the approximately 1.4 MB of DAS data generated each second.
- The processing of the data should be extended beyond the detection of the seismicity to include automatic picking, location and estimation of the origin time and magnitude. This aspect was not considered so far since the development of the infrastructure for data management was given first priority. A significant hindrance for source parameter determination using DAS stems in particular from the measurement type, as DAS produces strain-rate recordings (e.g. Lior et al., 2021). Nonetheless, the implementation of approaches applied to local seismicity monitoring in similar geo-reservoir contexts are currently investigated. Once the processing sequence is clearly

defined, optimizing the numerical tools (e.g. numerical codes, compilation) could also participate to the fast delivery of results.

Reducing the delay between the acquisition of data and the analysis of monitoring outcomes for near real-time characterization of the detected events constitutes a major aspect of the seismic monitoring of geo-reservoirs. For the field operator and the mining authorities, the objective is ultimately the mitigation of the induced seismicity, hence the combination of timely observations and model forecasts (Gaucher et al., 2022). More than a warning system, it should also help the operator to adapt the operation of the geothermal reservoir to minimize the risk associated with induced seismicity. The concept described here for DAS-based seismic monitoring is part of the development of such an integrated system.

Outlook for a reservoir management system

In order to minimize the induced seismicity risk and optimize the operational parameters, the real-time integration of monitoring outcomes and associated forecasts into the exploitation of geothermal sites is a critical aspect for the geothermal operators. At the SLS geothermal field, work on this issue has recently led to the concept of what would constitute a reservoir management system (RMS) (Gaucher et al. 2022). By merging seismic observations but also field production parameters and induced seismicity forecasts, the system should propose the geothermal field operator alternative production scenarios to mitigate the forecasted risks.

The system is composed of three main modules, which are linked and interact with each other (Gaucher et al. 2022). One of these modules, the database, is designed to gather the monitoring observations acquired in the field, the results of their processing, the operating parameters and the risk projections. The database is in interaction with the processing center, which is necessary to update the observational results and run forecasting numerical models. Finally, the dashboard synthesizes all available information with a finite number of key indicators and interfaces with the operators. The latter aims to facilitate decision-making based on modeled observations and predictions.

The monitoring system tested at the SLS geothermal site during the 6-months period demonstrates, with respect to the described RMS, the technical feasibility of acquiring, processing and archiving large amounts of data, as encountered with DAS. From this perspective, two major advantages of the proposed system are the scalability of the involved resources and the embedding in the operator's working environment. The latter, associated with the choice made with regard to the cloud service provider, aims at gathering the different modules of the RMS into a unified platform, routinely used by the operator. With respect to the scalability, the use of flexible cloud resources opens future perspectives for an extension of this concept to the processing of multiple physical quantities (including DAS, DTS and DSS data) and to the processing of data acquired on different geothermal sites and/or in multiple wells too.

Regarding DAS monitoring, expanding to multiple sites and/or wells would enable the combination of several measurement points, thereby addressing constraints linked to the utilization of a sole vertical DAS antenna (see Sect. "Monitoring capabilities of DAS along well"). For the SLS site, the cable deployed in the deviated well TH4 down to the

reservoir could be seamlessly integrated to the data management and processing environment. During the 6-months trial period, DAS recordings of the TH3 cable generated approximately 825 kB/s/km, with respect to the length of the interrogated fiber. Based on this value, the addition of the 3692-m long cable of TH4 would multiply by approximately three the rate of DAS data generated per second, reaching 4.4 MB/s. Whether this would be beneficial for induced seismicity monitoring should be evaluated in the future, since TH4 is a production well and the DAS cable is coupled to the casing by a sucker-rod. Nevertheless, the scalability of the system in place could easily support the additional volume of data to be transferred and processed. The cloud-based processing resources additionally provide ways to reduce processing times and to integrate more computationally demanding approaches, including the localization and the further characterization of the detected seismic events, which is subject to ongoing work.

Hence, the presented DAS monitoring set-up, implemented in a real operational environment, could be seen as a prototype for the RMS described in this section, that links the monitoring outcomes to the above-mentioned central database and uses some of the features of the processing center.

Conclusion

In this work, we describe the monitoring concept that has been developed to establish DAS as an effective component of the seismic monitoring of the Schäftlarnstraße geothermal field, located in the Munich inner city. The proposed concept links the on-site infrastructure, which includes the interrogated fiber and the DAS interrogator, to a cloud IoT platform. This cloud platform is designed to deliver both a secured storage environment for the DAS acquisitions and optimized IT resources for their processing. For mitigation purposes, we demonstrate the usability of the proposed concept to report on seismic event detections with low latency while processing minute-long data blocks.

The relevance of using DAS for seismic monitoring of an operating geothermal field is demonstrated by the observations collected during the 6-months testing period. First, the detection of a local event not visible from surface seismometers highlights that the sensitivity achieved is appropriate, even in conditions of high anthropogenic and operating noise (see Sect. "Spectral content of the DAS recordings"). Second, the DAS data quality is evidenced by the high spatial coherence observed for both P- and S-waves over the entire FOC, as well as the measured signal-to-noise ratio, especially for S-waves. The demonstrated level of sensitivity mostly results from the proximity of the downhole DAS sensors to the expected location of induced seismicity and from the application of detection (network coincidence) and de-noising (*f-k* filtering) techniques that take advantage of the high spatial and temporal sampling of the recordings. However, the monitoring configuration, featuring a single vertical FOC, limits the seismic source characterization, particularly with regard to determining its hypocenter. Thus, monitoring based on a single vertical DAS antenna cannot be considered as a standalone solution and additional monitoring tool(s) are necessary to provide complementary viewpoints.

The 6-months testing period and the related outcomes can be seen as a proof of concept, showing the viability of the proposed monitoring system and, thereby, the feasibility of acquiring continuous DAS data in geothermal wells under operational

conditions, while efficiently managing and processing the large and continuous flow of DAS recordings.

Finally, the flexibility of the proposed infrastructure concerning data storage capacity and high-performance processing resources opens perspectives for near real-time data processing and the further expansion of this concept to include additional monitoring components, e.g. DAS, seismometers but also field exploitation parameters. Hence, it could become the backbone of a reservoir management system designed to steer the exploitation of the geothermal reservoir in order to mitigate induced seismic hazard.

Abbreviations

DAS	Distributed acoustic sensing
DOFS	Distributed optical fiber sensors
DSS	Distributed strain sensing
DTS	Distributed temperature sensing
f-k	Frequency-wavenumber
FOC	Fiber optic cable
HDF5	Hierarchical Data Format version 5
IaaS	Infrastructure as a service
IoT	Internet of things
LTA	Long time average
OTDR	Optical time domain reflectometry
OMM	Obere Meeresmolasse
OSM	Obere Süßwasser Molasse
PaaS	Platform as a service
RAM	Random access memory
SAS	Shared access signature
SBM	Süßbrackwassermolasse
SLS	Schäftlarnstraße
SR	Strain-rate
SSD	Solid-state drive
STA	Short time average
TVD	True vertical depth

Acknowledgements
We would like to acknowledge the support of Shearwater in providing the seismic processing software Reveal©. We would like to express particular thanks to the IT-department of Stadtwerke München GmbH, and more particularly to Georg Aures, Maximilian Hansinger and Bettina Hille, for their support in setting up the accesses on the Azure account and managing the DAS data flow within the company's intranet. We also thank FEBUS Optics for their logistical support and the adjustment of the hardware of the A1-R interrogator to suit the needs expressed by this study. Finally, we would like to thank all the partners of the INSIDE project, Innovative Energie für Pullach GmbH, Erdwerk GmbH and Stadtwerke München GmbH, for their fruitful contribution to the INSIDE project.

Author contributions
JA designed the algorithms, performed the analysis and wrote the manuscript. EG contributed to the discussion, reviewed and edited the manuscript. KT coordinated the 6-months monitoring test for the geothermal operator (SWM) and reviewed the manuscript.

Funding
Open Access funding enabled and organized by Projekt DEAL. This work was conducted in the frame of the INSIDE project (https://inside-geothermie.de/en/inside-en/), which is supported by the German Federal Ministry for Economic Affairs and Climate Action and the Project Management Jülich (PtJ) under the grant agreement number 03EE4008C.

Availability of data and materials
The DAS strain-rate data for the two events studied and the Python scripts used on cloud work-stations for loading and processing the DAS data files are available at the following URL: https://publikationen.bibliothek.kit.edu/1000157458 (DOI: https://doi.org/10.5445/IR/1000157458).

Declarations

Competing interests
The authors declare no competing interests.

Appendix

See Figs. 8, 9, 10.

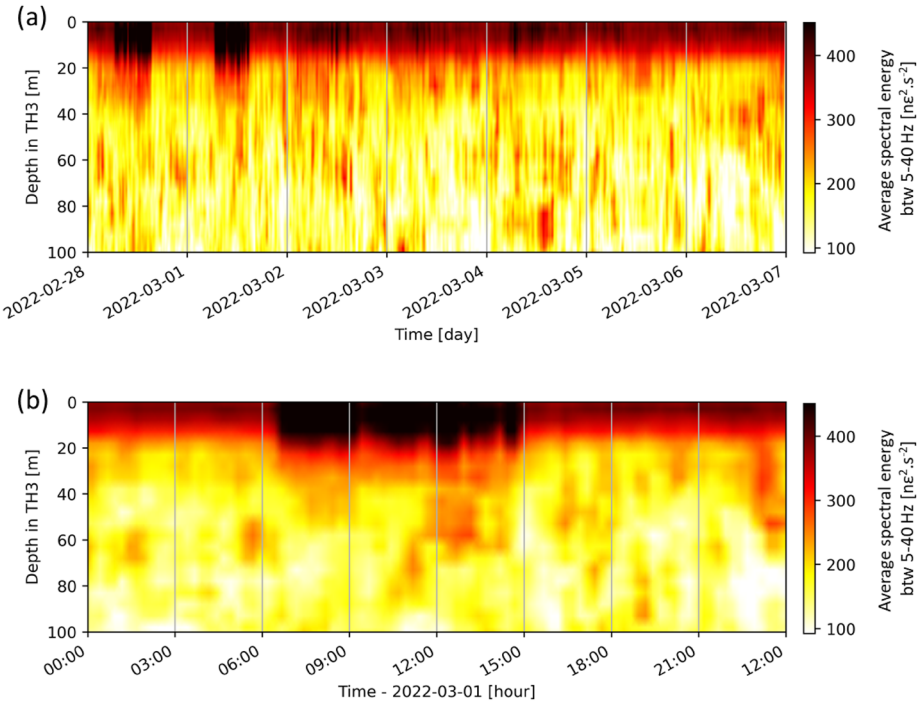

Fig. 8 Temporal and spatial variation of the average spectral energy of DAS recordings in the 5 to 40 Hz frequency band. From surface to 100 m (TVD), a power spectral density (PSD) is computed trace by trace and the spectral energy is averaged in the target frequency band. The average spectral energy is displayed as a function of depth and time over the course of a working week (panel (**a**), from Monday to Sunday) or over one full working day (panel (**b**), the 2022-03-01, Tuesday)

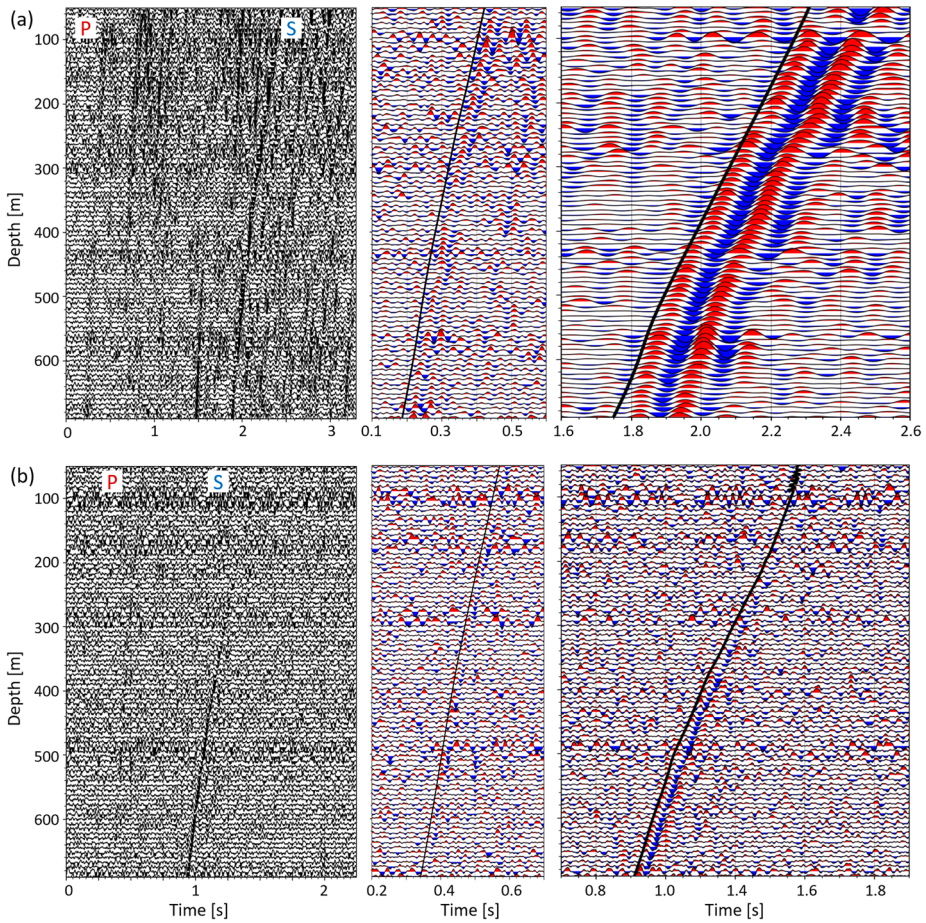

Fig. 9 Same as Fig. 6, without de-noising the strain-rate datasets in the f-k domain. Here, the data are only filtered between 5 and 40 Hz

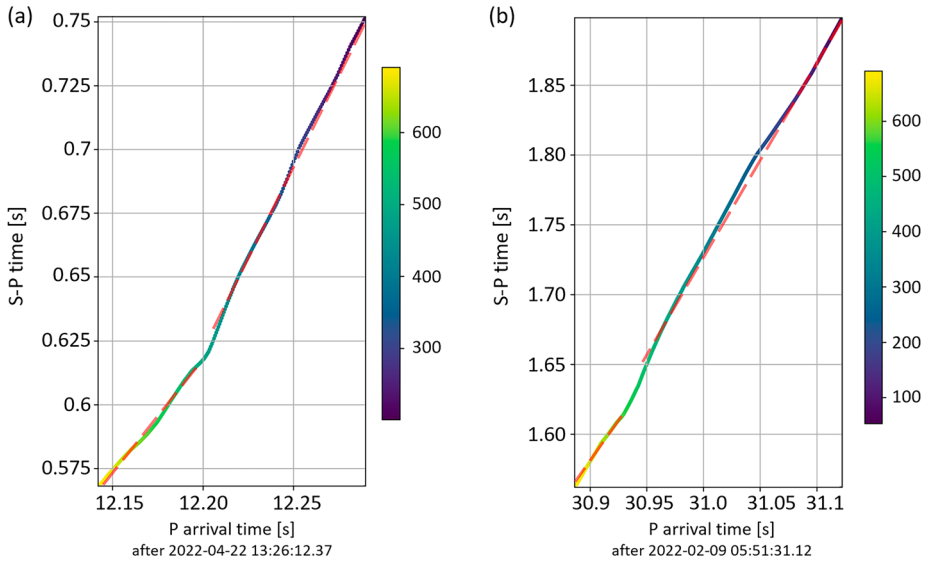

Fig. 10 Wadati diagrams computed using the P- and S-wave arrival times associated with the February [panel (**a**)] and the April [panel (**b**)] events. The color map shows the depth (TVD) of the sensing points along the TH3 fiber. The dashed lines in red show the linear regressions adapted to measurements below and above 500 m

Received: 22 May 2023 Accepted: 13 October 2023
Published online: 31 October 2023

References

Agemar T, Schellschmidt R, Schulz R. Subsurface temperature distribution in Germany. Geothermics. 2012;44:65–77. https://doi.org/10.1016/j.geothermics.2012.07.002.

Agemar T, Weber J, Schulz R. Deep Geothermal energy production in Germany. Energies. 2014;7(7):4397–416. https://doi.org/10.3390/en7074397.

Ajo-Franklin JB, Dou S, Lindsey NJ, Monga I, Tracy C, Robertson M, et al. Distributed acoustic sensing using dark fiber for near-surface characterization and broadband seismic event detection. Sci Rep. 2019;9(1):1328. https://doi.org/10.1038/s41598-018-36675-8.

Arbeitsgruppe „Induzierte Seismizität" des FKPE e.V.: Empfehlungen zur Überwachung induzierter Seismizität: Positionspapier des FKPE. 2012. https://www.fkpe.org/fileadmin/user_upload/Microsite_FKPE/dokumente/Induzierte_Seismizitaet/fkpe_ind_seis_monitor_120709_final.pdf

Azzola J, Gaucher E, Bögelspacher F, Ralph B, Betz B, Ilka S. INSIDE: Investigating the impact of geothermal exploitation in the Munich area. The induced seismicity perspective. 9th European Geothermal Workshop (EGW 2021), Karlsruhe, Deutschland. 2021. https://doi.org/10.5445/IR/1000152150.

Azzola J, Gaucher E, Ralph B, Ilka S. Deployment of a Distributed Fiber Optic Sensing (DFOS) monitoring station in Munich within INSIDE project. 82. Jahrestagung der Deutschen Physikalischen Gesellschaft (DGG 2022). 2022. https://doi.org/10.5445/IR/1000150919.

Baldwin CS. Brief history of fiber optic sensing in the oil field industry. SPIE Sensing Technology + Applications. 2014; doi: https://doi.org/10.1117/12.2050550.

Baldwin CS. Fiber optic sensors in the oil and gas industry: current and future applications. In: Alemohammad H, editor. Opto-Mechanical Fiber Optic Sensors. Butterworth-Heinemann; 2018. p. 211–36.

Beyreuther M, Barsch R, Krischer L, Megies T, Behr Y, Wassermann J. A python toolbox for seismology. Seismol Res Lett. 2010;81(3):530–3. https://doi.org/10.1785/gssrl.81.3.530.

Boer JJ den, Mateeva AA, Pearce JG, Mestayer JJ, Birch W, Lopez JL, et al. Detecting broadside acoustic signals with a fiber optical distributed acoustic sensing (DAS) assembly. 2017.

Böhm F, Savvatis A, Steiner U, Schneider M, Koch R. Lithofazielle reservoircharakterisierung zur geothermischen nutzung des malm im Großraum münchen. Grundwasser. 2013;18(1):3–13. https://doi.org/10.1007/s00767-012-0202-4.

Bohnsack D, Meinecke M, Thiemann K, Zosseder K, Gaucher E. 2023 Risk management of induced seismicity in the life cycle of a hydro-geothermal heating plant in an urban area. European Association of Geoscientists & Engineers. 84th EAGE Annual Conference & Exhibition. doi: https://doi.org/10.3997/2214-4609.2023101256

Bruno MS, Lao K, Oliver N, Becker M, California State University, Long BeachSilixa LLC. Use of Fiber Optic Distributed Acoustic Sensing for Measuring Hydraulic Connectivity for Geothermal Applications. 2018. doi: https://doi.org/10.2172/1434494

Correa J, Egorov A, Tertyshnikov K, Bona A, Pevzner R, Dean T, et al. Analysis of signal to noise and directivity characteristics of DAS VSP at near and far offsets—a CO2CRC otway project data example. Lead Edge. 2017. https://doi.org/10.1190/tle36120994a1.1.

Cröniger C, Tretter R, Eichenseer P, Kleinertz B, Timpe C, Bürger V, et al. Approach to climate neutral heat supply in munich 2035. Eur Geotherm Congr. 2022;2022:1–29.

Duncan G, Beresford G. Slowness adaptive f-k filtering of prestack seismic data. Geophysicists. 1994;59(1):140–7. https://doi.org/10.1190/1.1443525.

Dussel M, Lüschen E, Thomas R, Agemar T, Fritzer T, Sieblitz S, et al. Forecast for thermal water use from upper jurassic carbonates in the munich region (South German Molasse Basin). Geothermics. 2016;60:13–30. https://doi.org/10.1016/j.geothermics.2015.10.010.

Dzulhikam D, Rana ME. A Critical Review of Cloud Computing Environment for Big Data Analytics. International Conference on Decision Aid Sciences and Applications (DASA), Chiangrai (Thailand); 2022. doi: https://doi.org/10.1109/DASA54658.2022.9765168.

Farquharson N, Schubert DA, Steiner U. Geothermal energy in munich (and beyond) a geothermal city case study. GRC Transactions. 2016;40:189–96.

Gaucher E, Schoenball M, Heidbach O, Zang A, Fokker PA, van Wees J-D, et al. Induced seismicity in geothermal reservoirs: a review of forecasting approaches. Renew Sustain Energy Rev. 2015;52:1473–90. https://doi.org/10.1016/j.rser.2015.08.026.

Gaucher E, Hansinger M, Goblirsch P, Azzola J, Thiemann K. Towards a geothermal reservoir management system. European Geothermal Congress 2022, Berlin (Germany); 2022. https://doi.org/10.5445/IR/1000152177.

Grigoli F, Cesca S, Priolo E, Rinaldi AP, Clinton JF, Stabile TA, et al. Current challenges in monitoring, discrimination, and management of induced seismicity related to underground industrial activities: a European perspective. Rev Geophys. 2017;55(2):310–40. https://doi.org/10.1002/2016RG000542.

Haavik KE. On the use of low-frequency distributed acoustic sensing data for in-well monitoring and well integrity: qualitative interpretation. SPE J. 2023;28(03):1517–32. https://doi.org/10.2118/212868-PA.

Harris K, White D, Melanson D, Samson C, Daley TM. Feasibility of time-lapse VSP monitoring at the Aquistore CO2 storage site using a distributed acoustic sensing system. Int J Greenh Gas Control. 2016;50:248–60. https://doi.org/10.1016/j.ijggc.2016.04.016.

Hartog AH. An Introduction to Distributed Optical Fibre Sensors. 1st ed. Boca Raton: CRC Press; 2017.

Hartog A, Kotov OI, Liokumovich LB. The optics of distributed vibration sensing. Norway: Stavanger; 2013.

Isken MP, Vasyura-Bathke H, Dahm T, Heimann S. De-noising distributed acoustic sensing data using an adaptive frequency—wavenumber filter. Geophys J Int. 2022;231(2):944–9. https://doi.org/10.1093/gji/ggac229.

Jin G, Roy B. Hydraulic-fracture geometry characterization using low-frequency DAS signal. Lead Edge. 2017;36(12):975–80. https://doi.org/10.1190/tle36120975.1.

Johannessen K, Drakeley B, Farhadiroushan M. Distributed acoustic sensing—a new way of listening to your well/reservoir. SPE. 2012. https://doi.org/10.2118/149602-MS.

Juškaitis R, Mamedov AM, Potapov VT, Shatalin SV. Interferometry with Rayleigh backscattering in a single-mode optical fiber. Opt Lett. 1994;19(3):225. https://doi.org/10.1364/OL.19.000225.

Koelman JV. Fiber-optic sensing technology providing well, reservoir information—anyplace. Anytime J Pet Technol. 2011;63(07):22–4. https://doi.org/10.2118/0711-0022-JPT.

Koelman JM, Lopez JL, Potters JH. Optical fibers: the neurons for future intelligent wells. SPE Intell Energy Int. 2012. https://doi.org/10.2118/150203-MS.

Kraft T, Mai PM, Wiemer S, Deichmann N, Ripperger J, Kästli P, et al. Enhanced geothermal systems: mitigating risk in urban areas. EOS Trans Am Geophys Union. 2009;90(32):273–4.

Lellouch A, Yuan S, Ellsworth WL, Biondi B. Velocity-based earthquake detection using downhole distributed acoustic sensing—examples from the san andreas fault observatory at depth. Bull Seismol Soc Am. 2019;109(6):2491–500. https://doi.org/10.1785/0120190176.

Lellouch A, Lindsey NJ, Ellsworth WL, Biondi BL. Comparison between distributed acoustic sensing and geophones: downhole microseismic monitoring of the FORGE geothermal experiment. Seismol Res Lett. 2020;91(6):3256–68. https://doi.org/10.1785/0220200149.

Li Z, Zhan Z. Pushing the limit of earthquake detection with distributed acoustic sensing and template matching: a case study at the Brady geothermal field. Geophys J Int. 2018;215(3):1583–93. https://doi.org/10.1093/gji/ggy359.

Li M, Wang H, Tao G. Current and future applications of distributed acoustic sensing as a new reservoir geophysics tool. TOPEJ. 2015. https://doi.org/10.2174/1874834120150625E008.

Li Y, Karrenbach M, Ajo-Franklin JB. A Literature review distributed acoustic sensing in geophysics. Am Geophys Union (AGU). 2021. https://doi.org/10.1002/9781119521808.ch17.

Li D, Huang L, Zheng Y, Li Y, Wannamaker P, Moore J. Feasibility of source-free DAS logging for next-generation borehole imaging. Sci Rep. 2022;12(1):11910. https://doi.org/10.1038/s41598-022-16027-3.

Lindsey NJ, Rademacher H, Ajo-Franklin JB. On the broadband instrument response of fiber-optic DAS arrays. J Geophys Res Solid Earth. 2020. https://doi.org/10.1029/2019JB018145.

Lior I, Sladen A, Mercerat D, Ampuero J-P, Rivet D, Sambolian S. Strain to ground motion conversion of distributed acoustic sensing data for earthquake magnitude and stress drop determination. Solid Earth. 2021;12(6):1421–42. https://doi.org/10.5194/se-12-1421-2021.

Lomax A, Curtis A. Fast, probabilistic earthquake location in 3D models using oct-tree importance sampling. Dordrecht: Springer, Netherlands; 2001.
Lomax A, Virieux J, Volant P, Berge-Thierry C. Probabilistic earthquake location in 3D and layered models. In: Thurber CH, Rabinowitz N, editors. Advances in Seismic Event Location. Dordrecht: Springer, Netherlands; 2000.
Lomax A, Michelini A, Curtis A. Earthquake location, direct, global-search methods. In: Meyers RA, editor. Encyclopedia of Complexity and Systems Science. New York: Springer, New York; 2014.
Madsen K, Parker T, Gaston G. A VSP Field Trial Using Distributed Acoustic Sensing in a Producing Well in the North Sea. 74th EAGE Conference and Exhibition in Copenhagen (Denmark); 2012. https://doi.org/10.3997/2214-4609.20148801.
Martuganova E, Stiller M, Bauer K, Henninges J, Krawczyk CM. Cable reverberations during wireline distributed acoustic sensing measurements: their nature and methods for elimination. Geophys Prospect. 2021;69(5):1034–54. https://doi.org/10.1111/1365-2478.13090.
Masoudi A, Newson TP. Contributed Review: Distributed optical fibre dynamic strain sensing. Rev Sci Instrum. 2016;87(1):011501. https://doi.org/10.1063/1.4939482.
Mateeva A, Mestayer J, Cox B, Kiyashchenko D, Wills P, Lopez J, et al. Advances in Distributed Acoustic Sensing (DAS) for VSP. SEG Technical Program Expanded Abstracts 2012. Society of Exploration Geophysicists; 2012. p. 1–5. doi: https://doi.org/10.1190/segam2012-0739.1.
Mateeva A, Lopez J, Potters H, Mestayer J, Cox B, Kiyashchenko D, et al. Distributed acoustic sensing for reservoir monitoring with vertical seismic profiling: distributed acoustic sensing (DAS) for reservoir monitoring with VSP. Geophys Prospect. 2014;62(4):679–92.
Maurer V, Gaucher E, Grunberg M, Koepke R, Pestourie R, Cuenot N. Seismicity induced during the development of the Rittershoffen geothermal field, France. Geotherm Energy. 2020;8(1):5. https://doi.org/10.1186/s40517-020-0155-2.
McNamara DE. Ambient noise levels in the continental United States. Bull Seismol Soc Am. 2004;94(4):1517–27. https://doi.org/10.1785/012003001.
Megies T, Wassermann J. Microseismicity observed at a non-pressure-stimulated geothermal power plant. Geothermics. 2014;52:36–49. https://doi.org/10.1016/j.geothermics.2014.01.002.
Miller DE, Daley TM, White D, Freifeld BM, Robertson M, Cocker J, et al. Simultaneous Acquisition of Distributed Acoustic Sensing VSP with Multi-mode and Single-mode Fiber-optic Cables and 3C-Geophones at the Aquistore CO2 Storage Site. 2016;14.
Naldrett G, Cerrahoglu C, Mahue V. Production monitoring using next-generation distributed sensing systems. Petro S Journ. 2018;59(4):496–510. https://doi.org/10.30632/PJV59V4-2018a5.
Olofsson B, Martinez A. Validation of DAS data integrity against standard geophones—DAS field test at Aquistore site. Lead Edge. 2017;36(12):981–6. https://doi.org/10.1190/tle36120981.1.
Paitz P, Edme P, Gräff D, Walter F, Doetsch J, Chalari A, et al. Empirical investigations of the instrument response for distributed acoustic sensing (DAS) across 17 octaves. Bull Seismol Soc Am. 2021;111(1):1–10. https://doi.org/10.1785/0120200185.
Pankow K, Mesimeri M, Mclennan J, Wannamaker P, Moore J. Seismic Monitoring at the Utah Frontier Observatory for Research in Geothermal Energy. 45th Workshop on Geothermal Reservoir Engineering; Stanford University, Stanford, California; 2020.
Parker T, Shatalin S, Farhadiroushan M. Distributed Acoustic Sensing—a new tool for seismic applications. 2014;32:9.
Pickett GR. Acoustic character logs and their applications in formation evaluation. J Petrol Technol. 1963;15(06):659–67. https://doi.org/10.2118/452-PA.
Raab T, Reinsch T, Aldaz Cifuentes SR, Henninges J. Real-time well-integrity monitoring using fiber-optic distributed acoustic sensing. SPE J. 2019;24(05):1997–2009. https://doi.org/10.2118/195678-PA.
Reinsch T, Henninges J, Ásmundsson R. Thermal, mechanical and chemical influences on the performance of optical fibres for distributed temperature sensing in a hot geothermal well. Environ Earth Sci. 2013;70(8):3465–80. https://doi.org/10.1007/s12665-013-2248-8.
De Santis F, Klein E, Thoraval A, Contrucci I, Kinscher J. Case analysis of seismicity related to the exploitation of deep geothermal energy. European Geothermal Congress 2022, Berlin (Germany); 2022.
Schölderle F, Lipus M, Pfrang D, Reinsch T, Haberer S, Einsiedl F, et al. Monitoring cold water injections for reservoir characterization using a permanent fiber optic installation in a geothermal production well in the Southern German Molasse Basin. Geotherm Energy. 2021;9(1):21. https://doi.org/10.1186/s40517-021-00204-0.
Schulz R, Jobmann M. Hydrogeothermische Energiebilanz und Grundwasserhaushalt des Malmkarstes im Süddeutschen Molassebecken, Teilgebiet: Hydrogeothermik; Final Report. Institut für Geowissenschaftliche Gemeinschaftsaufgaben (GGA): Hannover, Germany. 1989;Archive Number 105040.
Seithel R, Gaucher E, Mueller B, Steiner U, Kohl T. Probability of fault reactivation in the bavarian molasse basin. Geothermics. 2019;82:81–90. https://doi.org/10.1016/j.geothermics.2019.06.004.
Soh J, Copeland M, Puca A, Harris M. Overview of Azure Infrastructure as a Service (IaaS) Services. In: Microsoft Azure: Planning, Deploying, and Managing the Cloud. Berkeley, CA: Apress; 2020a. p. 21–41. doi:https://doi.org/10.1007/978-1-4842-5958-0_2.
Soh J, Copeland M, Puca A, Harris M. Overview of Azure Platform as a Service. In: Microsoft Azure: Planning, Deploying, and Managing the Cloud. Berkeley, CA: Apress; 2020b. p. 43–55. doi:https://doi.org/10.1007/978-1-4842-5958-0_3.
Trnkoczy A. Understanding and parameter setting of STA/LTA trigger algorithm. 2012.
Van Der Horst J, Lopez JL, Berlang W, Potters H. In-Well Distributed Fiber Optic Solutions for Reservoir Surveillance. Offshore Technology Conference in Houston (Texas, USA); 2013. p. OTC-23949-MS. doi:https://doi.org/10.4043/23949-MS.
Wadati K, Oki S. On the Travel Time of Earthquake Waves. (Part II). Journal of the Meteorological Society of Japan. 1933;11(1):14–28. doi:https://doi.org/10.2151/jmsj1923.11.1_14
Wawerzinek B, Buness H, von Hartmann H, Tanner DC. S-wave experiments for the exploration of a deep geothermal carbonate reservoir in the German Molasse Basin. Geotherm Energy. 2021;9(1):6. https://doi.org/10.1186/s40517-021-00189-w.

Withers M, Aster R, Young C, Beiriger J, Harris M, Moore S, et al. A comparison of select trigger algorithms for automated global seismic phase and event detection. Bull Seismol Soc Am. 1998;88(1):95–106. https://doi.org/10.1785/BSSA0880010095.

Zhirnov AA, Stepanov KV, Chernutsky AO, Fedorov AK, Nesterov ET, Svelto C, et al. Influence of the laser frequency drift in phase-sensitive optical time domain reflectometry. Opt Spectrosc. 2019;127(4):656–63. https://doi.org/10.1134/S0030400X1910031X.

Publisher's Note